Fifty Years of Seismology of the Sun and Stars
ASP Conference Series, Vol. 478
K. Jain, S. C. Tripathy, F. Hill, J. W. Leibacher, and A. A. Pevtsov, eds.

Reflection and Refraction of (Magneto-)Acoustic Waves at the Magnetic Canopy: Further Evidences from Multi-Height Seismic Data

S. P. Rajaguru,[1] X. Sun,[2] K. Hayashi,[2] and S. Couvidat[2]

[1]*Indian Institute of Astrophysics, Koramangala II Block, Bangalore, India*
[2]*Hansen Experimental Physics Laboratory, Stanford University, Stanford, CA 94305, USA*

Abstract. We recently presented evidence (Rajaguru et al. 2013) that seismic halos around expanding magnetic structures in the lower solar atmosphere are related to the acoustic to magnetoacoustic wave conversions, using multi-height data from Helioseismic and Magnetic Imager (HMI) and Atmospheric Imaging Assembly (AIA: 1700 and 1600 Å channels) onboard *Solar Dynamics Observatory* (SDO). Using the same data, we present and discuss here further evidence through analyses of maps of phase-shifts between observables from different heights and their correspondence with oscillation power. The phase shift maps provide more direct signatures of reflection and refraction of (magneto-)acoustic wave modes.

1. Introduction

A rich variety of wave-dynamical phenomena in and around structured magnetic fields, large and small, that thread the solar atmospheric layers, are now amenable to detailed observational studies thanks to a variety of instruments, both space- and ground-based, that offer multi-line and mult-height measurements (see the review and references compiled by Khomenko & Calvo Santamaria 2013). Acoustic or seismic halos are regions of enhanced power, when compared to the quiet-Sun, surrounding strong-magnetic-field structures such as sunspots and plages at frequencies above the photospheric acoustic cut-off of ≈ 5.3 mHz, in the range of 5.5 – 7 mHz, and over regions of weak to intermediate strength (50 – 250 G) photospheric magnetic field (Braun et al. 1992; Brown et al. 1992; Hindman & Brown 1998) (see Rajaguru et al. 2013, for further references and a summary of existing observational and theoretical work). In our above referred recent work, through detailed analyses of power maps derived from photospheric Doppler velocity, continuum and line core intensities observed by the Helioseismic and Magnetic Imager (HMI; Scherrer et al. 2012) and that from upper photospheric and lower chromospheric UV emissions in the 1700 Å and 1600 Å wavelength channels imaged by the Atmospheric Imaging Assembly (AIA; Lemen et al. 2012) onboard the *Solar Dynamics Observatory* (SDO), we presented evidence that the seismic halos are related to the acoustic to magnetoacoustic wave conversion (Khomenko & Collados 2009). Here, using the same data sets, we analyse maps of phase-shifts between observables from different heights and their spatial correspondence with power maps as well as inclination and strength of magnetic field derived from HMI vector field observations.

2. Data and Analysis Method

The data sets used are the same as in Rajaguru et al. (2013, we refer the readers to this paper for details): 14-hour-long tracked data cubes of photospheric Doppler velocity [v], continuum intensity [I_c], line-core intensity [I_{co}], and dis-ambiguated vector magnetic field [B_x, B_y, and B_z] derived from HMI observations, and chromospheric UV emissions observed by AIA in the wavelength channels 1700 Å and 1600 Å, which we denote as I_{uv1} and I_{uv2}, respectively. The spatial extent of the region covered is 512 × 512 pixels, with a sampling rate of 0°.06 (heliographic) per pixel. In this paper we analyse the sunspot region NOAA 11092, whose central meridian passage was on 3 August 2010.

In addition to the power maps calculated as described in Rajaguru et al. (2013), we derive phase difference maps between the same physical variables. We analyse the spatial correspondence between power and phase maps through azimuthal averages (centered around the sunspot), and their relation to similarly averaged magnetic variables, total field strength and inclination.

3. Power and Phase Maps

The I_c, I_{co}, and v from HMI form at three different heights spread over $z = 0 - 300$ km above the continuum optical depth $\tau_c = 1$ ($z = 0$ km) level: I_c is from about $z = 0$ km, v corresponds to an average height of about $z = 140$ km (Fleck et al. 2011), and the line core intensity I_{co} corresponds to the top layer, at about $z = 280 - 300$ km, of the line formation region (Norton et al. 2006). The AIA 1700 Å and 1600 Å intensities [I_{uv1} and I_{uv2}] form at average heights of 360 km and 430 km (Fossum & Carlsson 2005), respectively. We have calculated phase shifts between all the intensities, ϕ_{I-I}, but for the purpose of this short presentation we present and discuss only those between I_c and [I_{co}, I_{uv1}]. Figure 1 displays the spatial maps of phase-shifts $\phi_{I_c-I_{co}}$ (left panel), and of phase shifts $\phi_{I_c-I_{uv1}}$ (right panel). Comparison of these phase shifts with the corresponding power maps from HMI Doppler v and AIA I_{uv1} in Figures 2 and 4 of Rajaguru et al. (2013) shows that regions of enhanced power correspond to a nulling of, or much, reduced phase shifts implying both upward and downward propagation in the layers between $z = 0$ to 300 km. All over the non-magnetic quiet region there is only upward propagation as shown by the uniform positive phase shifts: while for $\phi_{I_c-I_{co}}$ there is gradual increase in the phase shifts as frequency ν increases, $\phi_{I_c-I_{uv1}}$ display decreased values again at $\nu = 8$ mHz implying that such frequency waves begin to be evansecent (i.e., the cut-off frequency is reached) at heights where I_{uv1} forms. A closer examination of the spatial correspondence between power and phase variations is done through spotcentered azimuthal averages of power and phase shifts. These quantities are plotted in Figure 2 along with (in the bottom panels) similarly averaged magnetic quantities: total magnetic field strength B_{tot} and inclination γ with respect to the vertical direction. The left panel is for 6.0 mHz, and the right panel is for 8.0 mHz; solid curves show the phase shifts, while the dotted curves show the power normalised to quiet-Sun values. The horizontal dashed lines give the quiet-Sun average phase shifts, the horizontal dotted lines are at the normalised power level 1 (i.e., quiet-Sun level), and the two vertical dot-dashed lines mark the umbral (6.6 Mm) and outer-penumbral (17.5 Mm) radii. For heights less than about 300 km, as seen in the top two panels of Figure 2, there is a close correspondence between nulled, or much reduced, (as

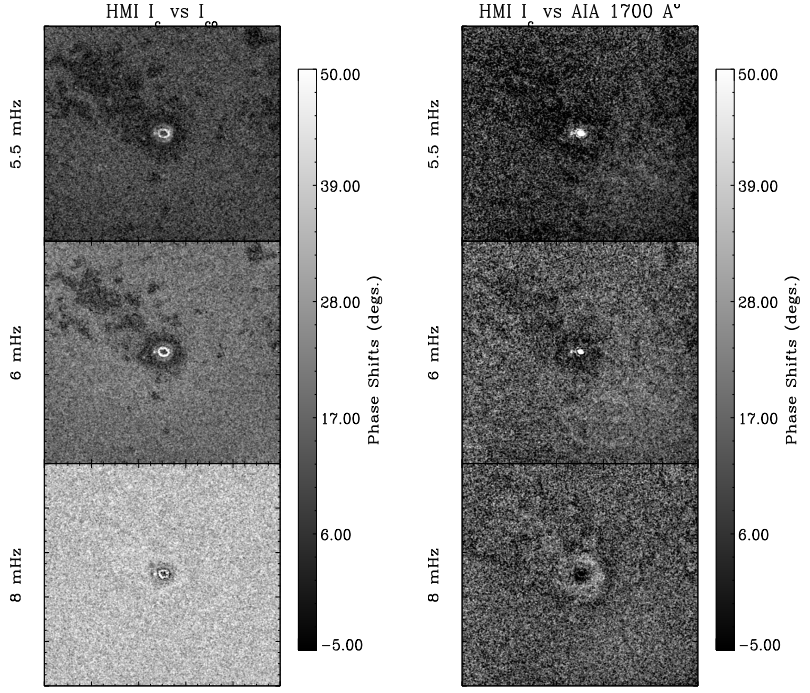

Figure 1. Maps of phase-shifts $\phi_{I_c-I_{co}}$ (left panel), and of phase shifts $\phi_{I_c-I_{uv1}}$ (right panel) over the sunspot region NOAA 11092 for three different frequencies as marked. The region shown here covers a square area of 373×373 Mm^2.

compared to quiet-Sun levels) phase shifts and the acoustic halos (or enhanced power) implying contributions from reflected or downward (following refraction) propagation of compressive waves. However, for acoustic halos at heights where AIA 1700 Å (I_{uv1}) form, there seem to be larger contributions from upward propagating waves.

Another interesting behaviour of phase and power variation is seen in the umbral and umbral-penumbral boundary region: above 5 mHz (here in the figure at 6 mHz) there is enhanced propagation between the height levels of I_c and I_{co} coinciding with highly suppressed power as seen in the intermediate level of Doppler v, while at higher levels this enhanced propagation 'migrates' to the the umbra and is the dominant propagation signal at 6 mHz as seen in the middle panel. It is to be noted that inclined B fields of penumbrae harbor propagating waves even at ν well below the photospheric cut-off of ≈ 5.2 mHz (not shown here; but have been studied in detail, e.g. in Rajaguru et al. 2010). However, at 8 mHz, there is a large negative phase shift showing downward propagation. We see this to be a possible result of refraction and reflection, above the umbral layers at heights above the formation heghts of I_{uv1}, of waves of 8 mHz. In fact, this downward propagation is observed to start at about 7 mHz (not shown in the figures).

More detailed analyses, including further results on phase shifts between other observables not shown and discussed here, are being prepared for a publication.

Acknowledgments. X. Sun, K. Hayashi, and S. Couvidat are supported by NASA grants NNG05GH14G to the SDO/HMI project at Stanford University. The data used here are courtesy of NASA/SDO and the HMI and AIA science teams.

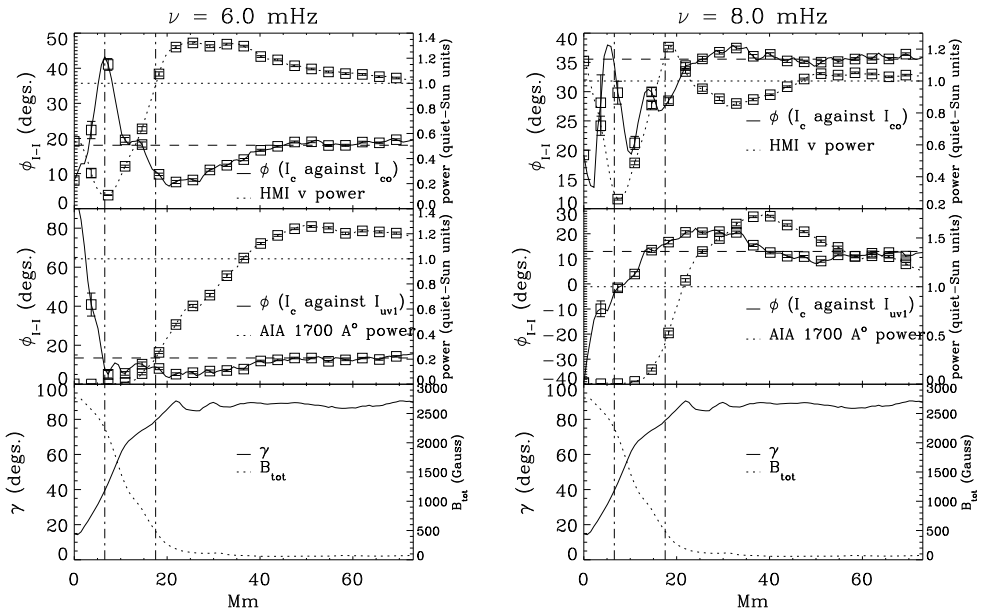

Figure 2. Azimuthal averages of normalised power and phase shift maps calculated between observables as marked in the panels. The bottom panels show the similarly averaged total magnetic field strength $B_{\rm tot}$ and inclination γ. Error bars depict the standard errors of the means plotted. Refer to the text for further details.

References

Braun, D. C., Lindsey, C., Fan, Y., & Jefferies, S. M. 1992, ApJ, 392, 739

Brown, T. M., Bogdan, T. J., Lites, B. W., & Thomas, J. H. 1992, ApJ, 394, L65

Fleck, B., Couvidat, S., & Straus, T. 2011, Solar Phys., 271, 27

Fossum, A., & Carlsson, M. 2005, ApJ, 625, 556

Hindman, B. W., & Brown, T. M. 1998, ApJ, 504, 1029

Khomenko, E., & Calvo Santamaria, I. 2013, J. Phys. Conf. Ser., 440, 012048

Khomenko, E., & Collados, M. 2009, A&A, 506, L5

Lemen, J. R., Title, A. M., Akin, D. J., Boerner, P. F., Chou, C., Drake, J. F., Duncan, D. W., Edwards, C. G., Friedlaender, F. M., Heyman, G. F., Hurlburt, N. E., Katz, N. L., Kushner, G. D., Levay, M., Lindgren, R. W., Mathur, D. P., McFeaters, E. L., Mitchell, S., Rehse, R. A., Schrijver, C. J., Springer, L. A., Stern, R. A., Tarbell, T. D., Wuelser, J.-P., Wolfson, C. J., Yanari, C., Bookbinder, J. A., Cheimets, P. N., Caldwell, D., Deluca, E. E., Gates, R., Golub, L., Park, S., Podgorski, W. A., Bush, R. I., Scherrer, P. H., Gummin, M. A., Smith, P., Auker, G., Jerram, P., Pool, P., Soufli, R., Windt, D. L., Beardsley, S., Clapp, M., Lang, J., & Waltham, N. 2012, Solar Phys., 275, 17

Norton, A. A., Graham, J. P., Ulrich, R. K., Schou, J., Tomczyk, S., Liu, Y., Lites, B. W., López Ariste, A., Bush, R. I., Socas-Navarro, H., & Scherrer, P. H. 2006, Solar Phys., 239, 69

Rajaguru, S. P., Couvidat, S., Sun, X., Hayashi, K., & Schunker, H. 2013, Solar Phys., 287, 107

Rajaguru, S. P., Wachter, R., Sankarasubramanian, K., & Couvidat, S. 2010, ApJ, 721, L86

Scherrer, P. H., Schou, J., Bush, R. I., Kosovichev, A. G., Bogart, R. S., Hoeksema, J. T., Liu, Y., Duvall, T. L., Zhao, J., Title, A. M., Schrijver, C. J., Tarbell, T. D., & Tomczyk, S. 2012, Solar Phys., 275, 207